

# Adjacent Tissues Reduce Shear Wave Speeds in Axially Loaded Tendons

Jonathon L. Blank<sup>1\*</sup>, Darryl G. Thelen<sup>1,2</sup>

<sup>1</sup>Department of Mechanical Engineering, University of Wisconsin-Madison, Madison, WI, USA

<sup>2</sup>Department of Biomedical Engineering, University of Wisconsin-Madison, Madison, WI, USA

## \* Correspondence:

Corresponding Author

[jlblank@wisc.edu](mailto:jlblank@wisc.edu)

**Keywords:** Tendon, subcutaneous fat, shear wave propagation, finite element model, multi-layered model, shear wave dispersion.

## Abstract

Shear wave tensiometry is a noninvasive approach for gauging tendon loads based on shear wave speed. Transient shear waves are induced and tracked via sensors secured to the skin overlying a superficial tendon. Wave speeds measured *in vivo* via tensiometry modulate with tendon load but are lower than that predicted by a tensioned beam model of an isolated tendon, which may be due to the added inertia of adjacent tissues. The objective of this study was to investigate the effects of adjacent fat tissue on shear wave propagation measurements in axially loaded tendons. We created a layered, dynamic finite element model of an elliptical tendon surrounded by subcutaneous fat. Transient shear waves were generated via an impulsive excitation delivered across the tendon or through the subcutaneous fat. The layered models demonstrated dispersive behavior with phase velocity increasing with frequency. Group shear wave speed could be ascertained via dispersion analysis or time-to-peak measures at sequential spatial locations. Simulated wave speeds in the tendon and adjacent fat were similar and modulated with tendon loading. However, wave speed magnitudes were consistently lower in the layered models than in an isolated tendon. For all models, the wave speed-stress relationship was well described by a tensioned beam model after accounting for the added inertia of the adjacent tissues. These results support the premise that externally excited shear waves are measurable in subcutaneous fat and modulate with axial loading in the underlying tendon. The model suggests that adjacent tissues do add inertia to the system, and hence must be considered when using tensiometry wave speed measures to infer absolute tendon loading.

## 1 Introduction

Shear wave tensiometry is an emerging technique for gauging tendon load based on the propagation speed of shear waves [1]. In tensiometry, an external actuator induces a transient wave in a superficial tendon. Skin-mounted accelerometers are used to track wave speeds in the underlying tissue. Wave speed can then be used to infer the axial loading in the tendon. Tensiometry can be performed at high repetition rates (e.g. 100 Hz), enabling the measurement of tendon wave speeds during dynamic movement such as walking and running [1]–[3].

The relationship between *in vivo* wave speed and tendon load is inherently complex. The finite thickness of tendon can also give rise to wave guided behavior, with wave propagation exhibiting dispersive behavior in which phase velocity depends on excitation frequency [4], [5]. A tensioned beam model [1] suggests that group wave speed in response to impulsive excitation depends on the tendon axial stress, tangential shear modulus, and the effective density of the tissue. Tendon is often modeled as a transversely isotropic material, in which fibers are embedded in a matrix and aligned in

the direction of loading. This structure results in a material that has high axial stiffness but a relatively low tangential shear modulus, due to the capacity of fibers to slide relative to each other. As a result, the axial stress in tendon becomes a dominant determinant of shear wave speed. Both finite element model predictions and *ex vivo* measurements are consistent with tensioned beam model predictions [6], [7]. In isolated tendon, wave speed varies in proportion to the square-root of axial stress, with speeds approaching 100 m/s with 15 MPa of axial stress [1].

Tensiometry measures of tendon wave speeds *in vivo* are considerably lower than those observed in isolated tendons. For example, Keuler et al. reported peak Achilles tendon wave speeds of 80 m/s during human walking, where the average stress is estimated to reach up to 40 MPa [8]. The lower wave speeds measured *in vivo* with tensiometry could arise from the added inertia effects of adjacent tissues. A prior study showed that tendon wave speeds in water are 22% lower than in air [7]. This difference was well predicted by the added inertia effects of the surrounding fluid. It is more challenging to predict the added inertia effects of the tissues (e.g., muscle and subcutaneous fat) that surround the tendon, or to assess how transient waves in the tendon might propagate through subcutaneous tissue to be detectable at skin-mounted sensors.

The objective of this study was to investigate the effects of adjacent tissues on shear wave propagation measurements in axially loaded tendons. To do this, we implemented a finite element model capable of simulating shear wave propagation patterns in a layered structure representing a tendon surrounded by subcutaneous fat. We simulated wave propagation generated via an ideal impulse in the tendon and by an external impulsive excitation through the layered structure, as done by current tensiometer devices [9]–[11]. We analyzed the dispersive nature of wave propagation in the tissues and compared group wave speed to that which would be obtained via temporal analysis of the transient waves. We expected to show that adjacent tissues decrease wave speed in axially loaded tendons, and that wave speeds measured at the tissue surface are similar to those propagating within the tendon.

## 2 Materials and Methods

### 2.1 Finite Element Model

#### 2.1.1 Overview

We developed a finite element model capable of simulating shear wave propagation [6], [12] in layered tissues. In the model, an elliptical tendon was enclosed in a subcutaneous fat medium. The subcutaneous fat and tendon layers were meshed using hexahedral elements. For a 60 mm long, 5 mm thick tendon with 3 mm of subcutaneous fat, the fat was composed of 12,960 elements and the tendon 2,250 elements. A mesh convergence analysis was performed in a prior finite element study and determined no changes in wave speed for a similar mesh pattern [6]. Contact between the outer surface of the tendon and inner surface of the subcutaneous fat was maintained using frictionless sliding-elastic contact. Surfaces were constrained such that the tendon and subcutaneous fat did not come out of contact during axial loading of the tendon. All finite element simulations were performed using FEBio v3.6.0 [13].

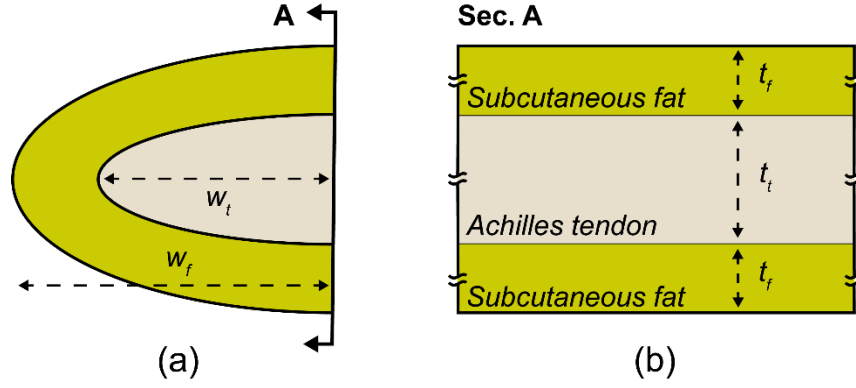


**Figure 1:** (a) The multi-layered finite element model included an elliptical tendon surrounded by subcutaneous fat. We assumed model symmetry on the right side. The tendon had a fixed width  $w_t$  of 5.5 mm, and the subcutaneous fat width was scaled based upon the ratio of fat to tendon present. (b) The tendon and subcutaneous fat were modeled with a thickness of  $t_t$  and  $t_f$ , respectively. The tendon and subcutaneous fat were modeled as 60 mm long. Specific variations in geometry are detailed in §2.4.1.

## 2.2 Constitutive Modeling

### 2.2.1 Tendon

We modeled the tendon as an incompressible, transversely isotropic hyperelastic material [14] that represents a tissue with longitudinal fibers embedded in a matrix using the following combination of strain energy density functions:

$$\Psi = \Psi_{matrix} + \Psi_{fibers} \quad (1)$$

Here,  $\Psi_{matrix}$  represents the contribution of the ground matrix and  $\Psi_{fibers}$  represents the contribution of embedded fibers. The ground matrix, embedded fibers, and tissue's volumetric response to loading were characterized using the following uncoupled strain energy density function,  $\Psi$ :

$$\Psi = F_1(\tilde{I}_1, \tilde{I}_2) + F_2(\tilde{\lambda}) + \frac{K}{2}(\ln J)^2 \quad (2)$$

$\tilde{I}_1$  and  $\tilde{I}_2$  represent the first and second invariants of the right Cauchy-Green deformation tensor,  $\tilde{\lambda}$  indicates the deviatoric part of the stretch ratio along the fiber direction,  $K$  represents the bulk modulus, and finally  $J$  represents the volume change of the deformation.  $F_1(\tilde{I}_1, \tilde{I}_2)$  represents the contribution of the ground matrix to the strain energy density function:

$$F_1(\tilde{I}_1, \tilde{I}_2) = C_1(\tilde{I}_1 - 3) + C_2(\tilde{I}_2 - 3) \quad (3)$$

We assumed the tissue constituted an isotropic, Mooney-Rivlin ground matrix [15]. The transverse tangential shear modulus of the ground matrix is estimated as  $2 \times (C_1 + C_2)$ .  $F_2(\tilde{\lambda})$  represents the contribution of the collagen fibers to the strain energy density function:

$$\tilde{\lambda} \frac{\partial F_2}{\partial \tilde{\lambda}} = 0 \quad \tilde{\lambda} \leq 1 \quad (4)$$

$$\begin{aligned}\tilde{\lambda} \frac{\partial F_2}{\partial \tilde{\lambda}} &= C_3 e^{C_4(\tilde{\lambda}-1)} - 1 & 1 < \tilde{\lambda} \leq \lambda^* \\ \tilde{\lambda} \frac{\partial F_2}{\partial \tilde{\lambda}} &= C_5 \tilde{\lambda} + C_6 & \tilde{\lambda} > \lambda^*\end{aligned}$$

Here,  $\tilde{\lambda}$  represents the axial tissue stretch during loading and  $\lambda^*$  is the stretch at which the fibers engage. In the toe region,  $C_3$  scales the exponential stress and  $C_4$  scales the strain-dependent rate at which the fibers uncrimp.  $C_5$  is the elastic modulus of straightened fibers and  $C_6$  is set so that the stress-strain curve is continuous at  $\lambda^*$ . For a transversely isotropic material with perfectly aligned fibers, as is presented here, the stretch of the collagen fibers is the same as the axial stretch,  $\tilde{\lambda}$ . We chose constitutive parameter values based on previous finite element modeling studies of transversely isotropic tendons and ligaments [6], [16], [17].

### 2.2.2 Subcutaneous Fat

We modeled the subcutaneous fat as a nonlinear, anisotropic, and uncoupled Ogden material [18]. The hyperelastic strain energy function is given by the following:

$$\Psi = \sum_{i=1}^N \frac{\mu_i}{\alpha_i} (\lambda_1^{\alpha_i} + \lambda_2^{\alpha_i} + \lambda_3^{\alpha_i} - 3) + U(J) \quad (5)$$

Here,  $\mu$  and  $\alpha$  represent material constants, and  $\lambda_{1-3}$  represent the deviatoric principle stretches. The term  $U(J)$  is the volumetric component and  $J$  is the deformation gradient of the subcutaneous fat material. The undeformed shear modulus of the material in the stress-free configuration is given by the following relationship:

$$\sum_{i=1}^N \mu_i \alpha_i = 2\mu \quad (6)$$

We applied Ogden material parameters based on a prior study that characterized the multidirectional properties of subcutaneous fat and satisfied the constraints that  $\mu$  was positive and  $\lambda_1 \lambda_2 \lambda_3 = 1$ . [19].

**Table 1:** Constitutive parameters used in the transversely isotropic tendon and Ogden subcutaneous fat.

Transversely Isotropic (tendon)		Ogden (subcutaneous fat)	
Density, $\rho$ [kg/m <sup>3</sup> ]	1500	Density, $\rho$ [kg/m <sup>3</sup> ]	1000
$C_1$ [MPa]	2.05	$\mu_1$ [kPa]	$2.18 \times 10^4$
$C_2$ [MPa]	2.05	$\mu_2$ [kPa]	$1.04 \times 10^{-1}$
$C_3$ [MPa]	1	$\mu_3$ [kPa]	$-2.81 \times 10^3$
$C_4$	50	$\alpha_1$	$3.36 \times 10^{-2}$
$C_5$ [MPa]	$6 \times 10^2$	$\alpha_2$	16.4
$\lambda^*$ [mm/mm]	1.04	$\alpha_3$	$2.58 \times 10^{-1}$
K [MPa]	$10^3 \times C_1$	K [MPa]	5

### 2.3 Shear wave propagation simulation

### 2.3.1 Shear wave excitation techniques

#### 2.3.2 Dynamic simulation of wave propagation

Tendons were axially loaded by displacing the proximal cross-section of the tendon in the axial direction with the distal end held fixed. We applied displacements that induced axial strains ranging from 0 to 10%. We excited the shear wave in the multi-layered model using an impulsive excitation applied across the entire cross-section (idealized) and via an external contact through the subcutaneous fat (external), as is used commonly *in vivo* [20]. The idealized excitation was performed by displacing nodes at the proximal end of the tendon transversely. The external excitation was performed using a rigid mechanical tapper in contact with the superficial surface of the subcutaneous fat (frictionless sliding-elastic contact). The rigid tapper was pressed into the subcutaneous fat by  $0.5t_f$  prior to the impulsive excitation being applied (Fig. 1). For both the idealized and external excitation, the excitation displacement profile was a half sine with a half period of  $250 \mu\text{s}$  with an amplitude of  $100 \mu\text{m}$ . The resulting shear wave in the tendon-subcutaneous fat structure was simulated for 2.5 ms (Fig. 2).

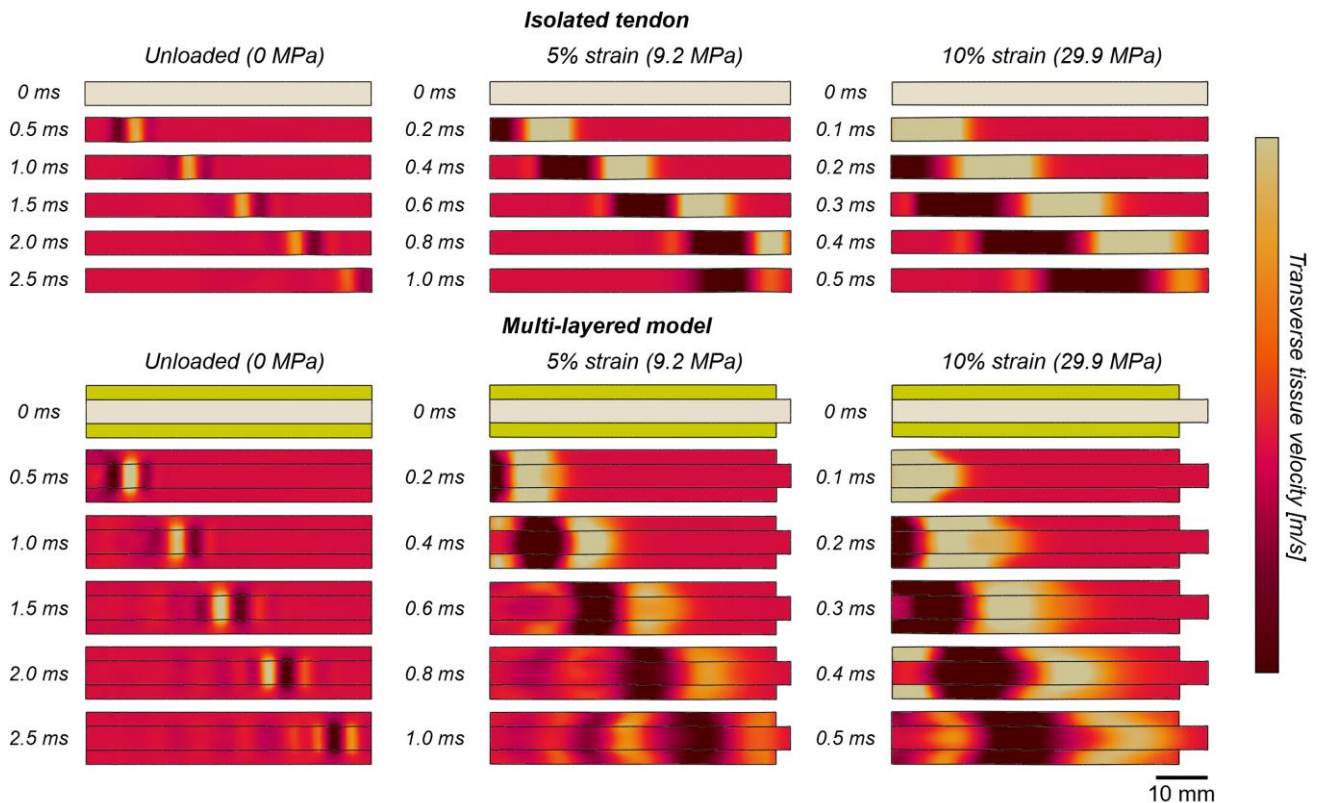


**Figure 2:** Shear wave propagation patterns in an isolated tendon and in the multi-layered model. Shear wave propagation patterns displayed were the result of an idealized excitation. Shear waves in the model propagate faster when the tendon is loaded, and wave propagation in the model (as indicated by the transverse velocity colormap) is observed in both the tendon and subcutaneous fat.

#### 2.3.3 Transient shear wave speed measurement

Tendon wave speed was assessed based on the transverse motion of nodes along the central axis of the tendon, the tendon-superficial fat interface, and along the surface of the superficial fat. For ideally excited simulations, shear wave speeds were measured using the best fit slope of the distance between transverse motion peaks and their time delay in wave arrival (in m/s) (Fig. 3a). For externally excited simulations, the shear wave speed was determined using a cosine-interpolated,

normalized cross-correlation between the transverse motion of two nodes with cosine interpolation to assess sub-sample alignment [21], as is done *in vivo*. Shear wave speed for these simulations was then computed as the distance between measurement nodes divided by the calculated time delay. Axial tendon stress was computed using the average axial stress across measurement regions.

### 2.3.4 Shear wave dispersion analysis

We performed a 2D fast Fourier transform-based (2D FFT) dispersion analysis on our dynamic models to assess the effects of subcutaneous fat on the frequency content of the shear wave propagation [4], [22]–[24]. Briefly, we reconstructed the spatiotemporal profile of the shear wave propagation at a fixed depth in the model (Fig. 3a). For the dispersion analysis we used ideally excited shear wave propagation along the entire length of the tendon (i.e., 60 mm). We first applied a linear interpolation to the spatiotemporal profile of the shear wave to increase the density of phase velocity points. We then applied a 2D FFT to the spatiotemporal profile to extract the temporal frequency (in Hz) and spatial frequency (in  $\text{m}^{-1}$ ) of the propagated shear wave in  $k$ -space (Fig. 3b). Finally, the phase velocity is given by:

$$c_p = \frac{f}{k} \quad (7)$$

where  $f$  is the temporal frequency (in Hz),  $k$  is the wavenumber (i.e., spatial frequency) (in  $\text{m}^{-1}$ ), and  $c_p$  is the phase velocity (in m/s). We identified the maximum intensity at each temporal frequency represented in the  $k$ -space diagram and used linear regression to determine a slope between temporal frequency and wavenumber. We then converted our  $k$ -space intensities to phase velocity to visualize the dispersion curve (Fig. 3c), where the phase velocity converges to the group speed of the observed wave packet at high frequencies. The phase velocities from the shear wave excited were extracted using the phase velocity transform of the maximum observed intensities in the  $k$ -space diagram (Fig. 3d). For ideally excited simulations, we computed the group shear wave speeds and compared to those measured using the transient, slope-based approach outlined in §2.3.3.

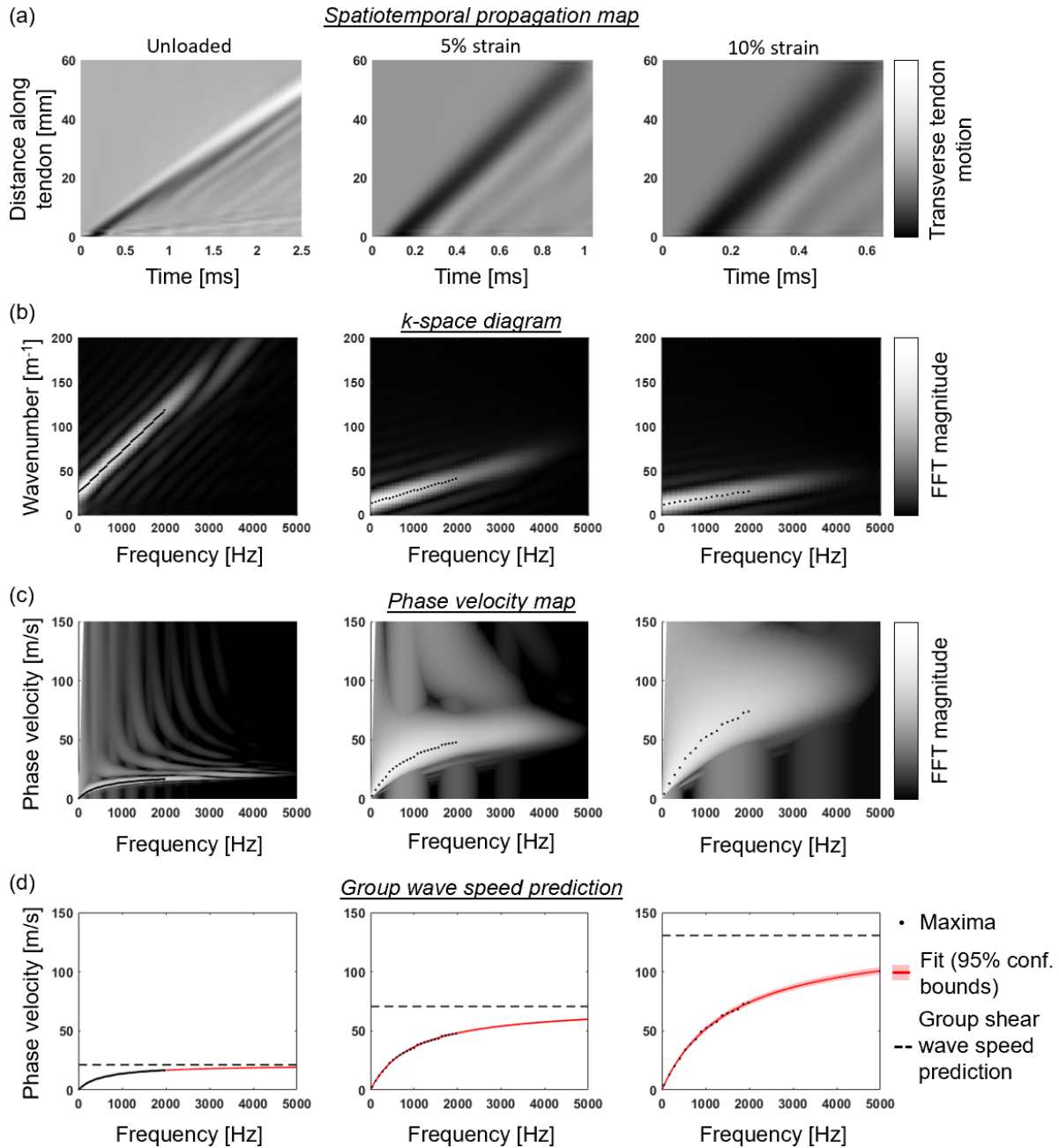


**Figure 3:** (a) The shear wave was allowed to propagate along the length of the 60 mm tendon embedded in subcutaneous fat. (b) We performed a 2D FFT on the spatiotemporal shear wave profile from (a). (c) We extracted phase velocity as a function of temporal frequency using Equation 7. (d) We used a linear fit (in the spatiotemporal frequency domain) to determine phase velocity as a function of temporal frequency and the group velocity of the shear wave. Dispersion analysis was performed for simulations using an idealized excitation only.

## 2.4 Sensitivity analyses

### 2.4.1 Sensitivity to tendon and subcutaneous fat geometry

We assessed the sensitivity of our model to tendon and subcutaneous fat thickness by creating 12 models of tendon thicknesses spanning 3, 5, and 7 mm, and subcutaneous fat thicknesses spanning 1,

3, and 5 mm (including isolated tendon) (Fig. 1b). The tendon width was held fixed at 5.5 mm for all simulations (Fig. 1a), and the subcutaneous fat width was scaled to the width needed to achieve a thickness variation of 2 mm. Tendon axial load was modulated by varying the axial tendon strain for 0-10% according to a uniform distribution. All variations in geometry were evaluated using ideal excitations and 1,000 simulations per geometry were performed on a high-throughput computing grid to assess changes in shear wave speed with tendon loading.

#### 2.4.2 Sensitivity to excitation technique

We evaluated variations in excitation (idealized, external) techniques by creating two separate base models. For the external excitation, we displaced the tapper into the layered structure by 1.5 mm. Comparisons between excitation techniques were evaluated for a model with a tendon thickness of 5 mm and a subcutaneous fat thickness of 3 mm (Fig. 1b). Tendon axial load was modulated by varying the axial tendon strain from 0-10% according to a uniform distribution. We performed 500 simulations per condition on a high-throughput computing grid to assess changes in shear wave speed with tendon loading.

### 2.5 Statistical analysis

We assessed the shear wave speed-axial stress relationship using the tensioned beam model for shear wave tensiometry [1], [25]:

$$\sigma = \rho_{eff}c^2 - k'\mu \quad (8)$$

Here,  $\sigma$  represents the axial tendon stress (in Pa),  $\rho_{eff}$  the effective density of the propagation medium (in  $\text{kg/m}^3$ ),  $c$  the shear wave speed (in m/s),  $k'$  a shear correction factor (unitless), and  $\mu$  the tangential shear modulus of the tendon (in Pa). We used linear regression to assess the correspondence of model results to our tensioned beam model and to compare the effective density of the system across geometries. For all linear regressions, the dependent variable was the axial stress,  $\sigma$ , and the independent variable was the squared shear wave speed,  $c^2$ .

## 3 Results

### 3.1 Presence of subcutaneous fat lowers tendon shear wave speeds

Shear wave speeds in the tendon increased with increasing tendon strain (Fig. 4a). For isolated tendon, shear wave speeds corresponded well with a tensioned beam model in which the effective density is attributable solely to the tendon tissue. For the layered models, shear wave speeds were substantially lower but modulated with tendon stress in a manner that could be described by a tensioned beam model. Numerical estimates of effective tissue density were sensitive to the amount of tendon and subcutaneous fat present in the model. Namely, there was an increase in the effective density of the system for a constant tendon thickness when the thickness of the subcutaneous fat increased (Fig. 4b). Shear wave speed-axial stress relationships for all geometry combinations can be found in the Electronic Supplementary Material (Fig. 1S).

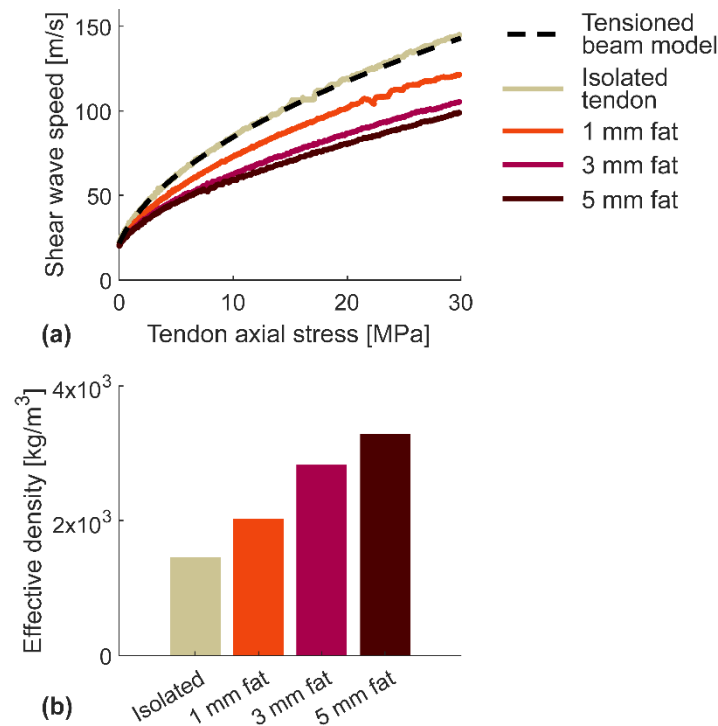


**Figure 4:** (a) Tendon-measured shear wave speeds were sensitive to the geometry of the tendon and subcutaneous fat, with lower shear wave speeds being measured in models with less subcutaneous fat. Isolated tendon shear wave speeds were in range of the tensioned beam model. (b) The effective density of the model increased with an increasing subcutaneous fat thickness.

### 3.2 Layered shear wave dispersion affects shear wave speed-stress calibration

Phase velocity of the shear wave increased monotonically with axial stress and temporal frequency (Fig. 5a). Phase velocity magnitudes asymptotically approached the group shear wave speed at higher frequencies. Our measure of group shear wave speed based on the linear fit in  $k$ -space agreed well with our transient measured of shear wave speed made within the tendon (Fig. 5b).

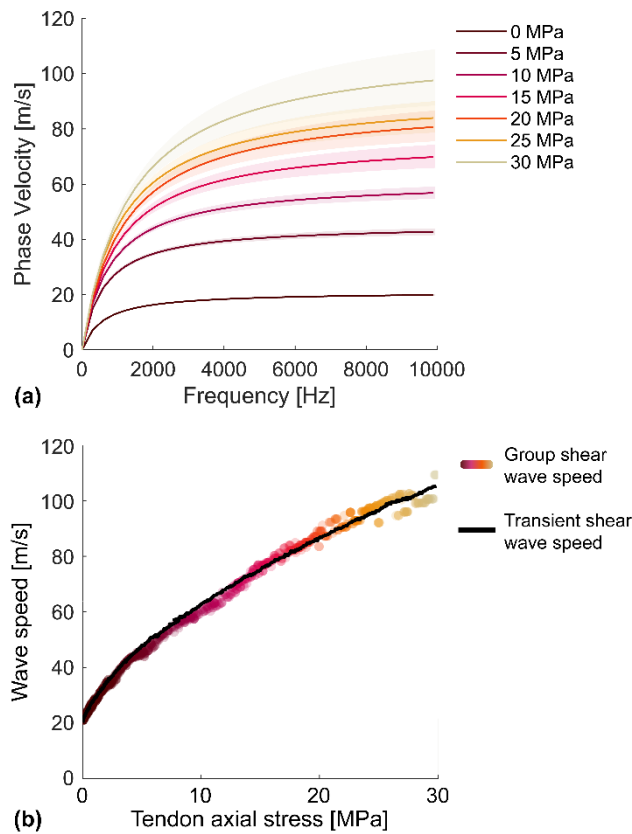


**Figure 5:** (a) Phase velocity increased monotonically with frequency and approached the group velocity asymptotically. Shaded regions indicate 95% confidence bounds on the  $k$ -space linear fit. (b) Group wave speed computed using a dispersion analysis agreed well with the transient shear wave speeds induced via an impulsive excitation.

### 3.3 Shear wave propagation, dispersion, and speed are sustained within the superficial fat

A consistent shear wave speed-axial stress relationship was evident in both the tendon and adjacent tissues. For example, similar wave speeds were determined when analyzing nodal displacements along the tendon midline, at the superficial surface of the tendon, and at the superficial surface of the fat (Fig. 6). We also observed that frequency-dependent dispersion patterns were maintained at these measurement locations (group velocity shown in Fig. 6).

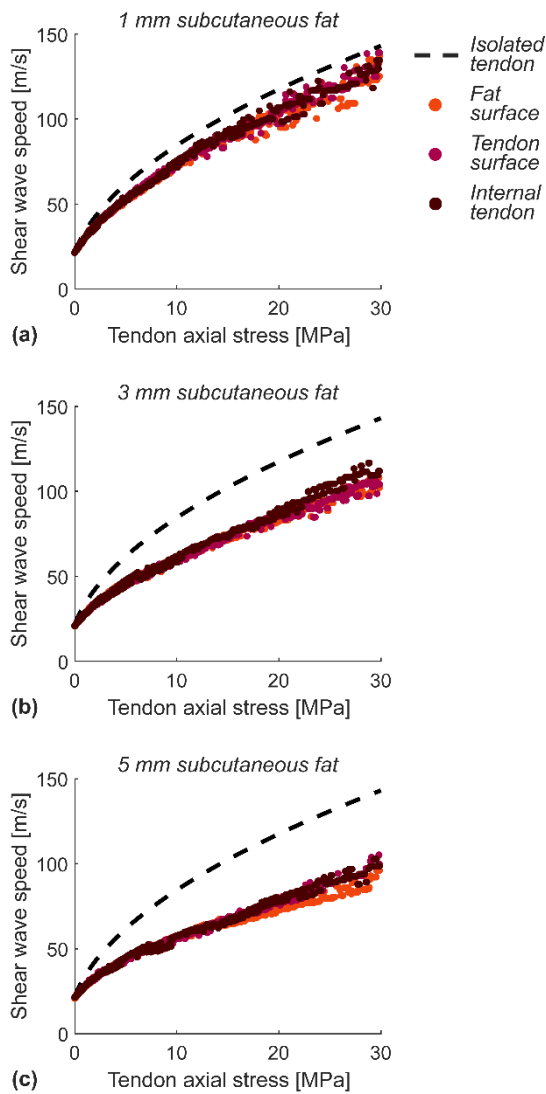


**Figure 6:** Shear wave propagation was monitored at the fat surface, at the tendon surface, and within the tendon. Independent of the amount of subcutaneous fat present, shear wave speeds (measured using group speed) and dispersion patterns were similar between measurement regions. All results shown are for a tendon thickness of 5 mm.

### 3.4 External excitations can excite shear waves within the tendon

Shear waves excited via an external impulsive excitation induced waves within the tendon that also modulated with loading (Fig. 7a). When subcutaneous fat was present, externally excited shear waves were less distinct than achieved using the ideal excitation (Fig. 7b vs Fig. 3a). However, transient shear wave speeds could still be ascertained from time-to-peak measures obtained at sequential spatial locations along the fat or tendon. External excitation did induce slightly lower wave speeds, which resulted an effective density estimate that was slightly higher than that observed via an ideal excitation.

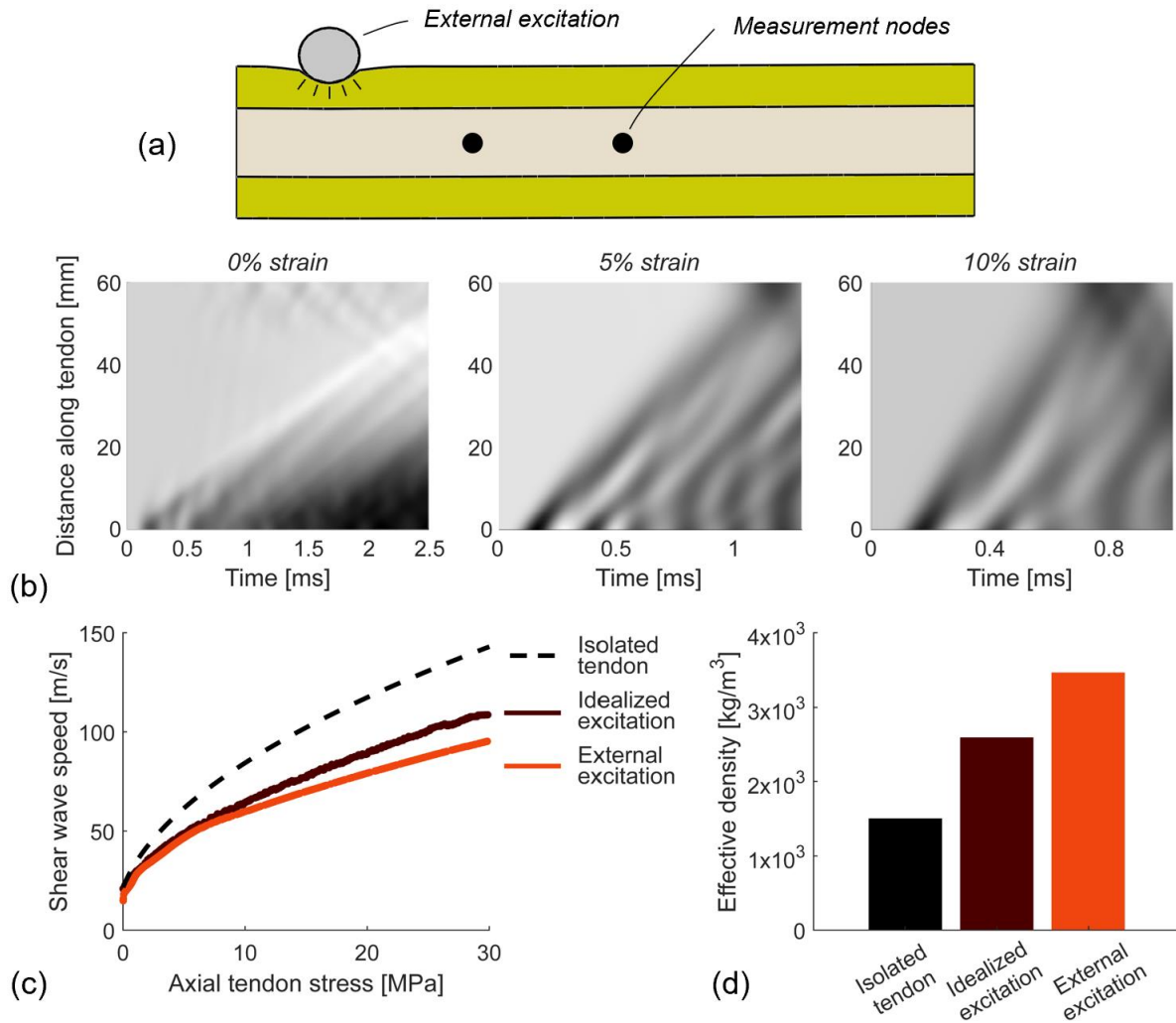


**Figure 7:** (a) External shear wave excitations featured a rigid tapper in contact with the superficial surface of the subcutaneous fat. (b) Shear wave propagation could be ascertained via spatial displacement images in both the unloaded and loaded tendons. (c) Externally excited shear wave speeds modulated in proportion to the square-root of axial tendon stress, albeit with lower speeds than seen in the isolated tendon. (d) The estimated effective density for externally excited shear wave speeds was greater than the tendon density, and slightly higher than the effective density measured using an idealized excitation.

#### 4 Discussion

The objective of this study was to investigate the effects of adjacent tissues on shear wave propagation in axially loaded tendons. To do this, we developed a multi-layered finite element model of an elliptical tendon surrounded by subcutaneous fat of varying thicknesses. We found that the presence of adjacent subcutaneous fat increased the effective density of the vibrating tendon, and hence produced slower waves speeds than observed in isolated tendon. However, the wave speed-stress relationship was still well approximated by a tensioned beam model, albeit with an effective density that depended on the relative amounts of subcutaneous fat and tendinous tissue. The layered models did exhibit dispersive behavior, with the phase velocity approaching the group velocity at excitation frequencies between 1000 and 10,000 Hz. These results can inform further development and use of noninvasive tensiometers for characterizing tendon loads *in vivo*.

A primary observation of our study was that adjacent fat reduced the apparent shear wave speed in tendon. For example, by varying the amount of subcutaneous fat alone, we observed nearly a two-fold increase in the effective density of the system (Fig. 4). These results are consistent with a prior *ex vivo* study showing that tendon waves travel 22% slower when vibrating in water than when vibrating in air. The subcutaneous fat layer reduced shear wave speeds further than water, which may be the cause of additional effects imposed by a solid medium (i.e., material properties). We also demonstrated sensitivity of tendon-measured shear wave speed to adjacent tissue inertia by varying the amount of subcutaneous fat density present. While we expect that the mass density of subcutaneous fat in human subjects would be relatively constant [26], [27], there could be variations in shear wave speed in human subjects due to relative amounts of subcutaneous fat present (and thus, a higher mass of adjacent tissues). It may be possible to correct for such factors by using imaging (e.g., MRI or ultrasound) to characterize the geometry of tendon and adjacent tissues. Larger scale human subject studies would be needed to characterize whether such a calibration procedure can account for variability in the wave-speed stress relationship across subjects [2].

Our simulations demonstrate the presence of dispersion in the layered tissue model. Notably, phase velocity increased with frequency and asymptotically approached the group velocity at frequencies ranging from 1000 to 10,000 Hz (Fig. 5a). The dispersive behavior likely arises from the finite thickness of tendons, which results in wave guided behavior at lower frequencies [4]. While high-frame rate ultrasonic imaging approaches can be used to measure dispersive behaviors in tissues [5], it is not feasible in tensiometry which, limited to the use of sparse spatial measures to characterize wave propagation. However, we show that transient impulsive excitations (250  $\mu$ s pulse) can produce a wave speed that approaches the group wave speed ascertained via dispersion analysis. Further human subject testing with different excitation patterns in tensiometry are warranted to better understand the nature of dispersion *in vivo*, and how to properly account for excitation frequencies when using skin-based measures of wave speed to infer tendon loading.

We were able to excite a shear wave measurable within both the tendon and subcutaneous tissue using external impulsive actuation. While shear wave propagation patterns were more complex than observed with an idealized planar excitation, it remained feasible to track load-dependent variations in wave speed via sparse, transient measurements within the tendon. The resulting wave speed-stress relationships were generally consistent between the ideally and externally excited conditions. While this result is promising, further sensitivity analyses and experimental validation of the external excitation condition are warranted. Additional parameters to consider are the external excitation pattern, the pre-load of the device into the skin, and the relative location of the sensors used to monitor wave propagation [12].

There are prior studies that examined shear wave propagation patterns in layered structures. Sadeghi and Cortes examined shear wave propagation in thin-layered agarose gel phantoms using ultrasound [28], measuring shear wave speeds that resulted in a more accurate prediction of shear modulus in the tissue of interest. Further, they clarify that the same or similar methods could be used to obtain a more accurate measure of shear wave speed in a subcutaneous tissue, as was investigated in this study. Second, Nguyen et al. studied the quantification of shear modulus in a layered organ model using a simulated supersonic shear imaging technique (shear wave spectroscopy) [29]. They observed strong guided wave behavior along the thin-layered organ, which corroborates our findings of dispersion within this layered model. These relatively recent studies, in concert with the findings presented here, suggest that accounting for adjacent tissues is of increasing importance if one is to correctly quantify loading or material properties in soft tissues *in vivo* using shear wave propagation.

There are limitations to consider when interpreting these results. First, we used simplified geometries to construct the tendon and subcutaneous fat layers. Anatomical geometries that include more detailed morphology of the tendon (e.g., subject-specific anatomy or with subtendons [30]) and subcutaneous fat may reveal further important relationships between tendon measured shear wave speeds and surrounding adjacent tissues. Second, we primarily investigated inertial effects of wave propagation and measurement techniques, but there may be other mechanisms that alter shear wave propagation, such as variation in adjacent tissue material properties and types of adjacent tissues (i.e., subcutaneous fat, muscle, bone, skin). More specifically, this model should be further adapted to provide a more detailed insight into shear wave propagation in other tissues relevant for tensiometry applications, such as in ligaments [31] which have a shorter span between bony attachments. Finally, subcutaneous fat material properties are viscoelastic in addition to being nonlinear and anisotropic [32]. Future studies using this layered propagation model should investigate its sensitivity to both the elastic and viscoelastic material properties of subcutaneous fat and other adjacent tissue types.

In summary, we developed a layered finite element model capable of predicting tendon shear wave speeds that are similar in magnitude to those observed *in vivo* [2]. The presence of adjacent tissues, in this case subcutaneous fat, increase the effective inertia of the system and reduce shear wave propagation speeds. The new knowledge provided in this study allows for more nuanced interpretations of tendon loading measurements made using shear wave tensiometry and advances the fidelity of models for understanding shear wave propagation patterns *in vivo*.

## 5 Conflict of Interest

*The authors declare that the research was conducted in the absence of any commercial or financial relationships that could be construed as a potential conflict of interest.*

## 6 Author Contributions

JB, DT: conceptualization, writing - review and editing, funding acquisition. JB: original draft preparation, model development, model analysis. DG: supervision.

## 7 Acknowledgments

The authors would like to acknowledge the University of Wisconsin-Madison Center for High-Throughput Computing for their resources and technical insight related to this project. We also thank Eli Dawson, Dylan Schmitz, and Matt Allen for valuable discussions on wave propagation in layered structures.

This material is based upon work supported by NIH Grant No. HD092697 (D.G.T.) and the National Science Foundation Graduate Research Fellowship Program under Grant No. DGE1747503 (J.L.B.). Any opinions, findings, and conclusions or recommendations expressed in this material are those of the author(s) and do not necessarily reflect the views of the National Science Foundation.

## 8 References

- [1] J. A. Martin *et al.*, “Gauging force by tapping tendons,” *Nat. Commun.*, vol. 9, no. 1, pp. 2–10, 2018, doi: 10.1038/s41467-018-03797-6.
- [2] E. M. Keuler, I. F. Loegering, J. A. Martin, J. D. Roth, and D. G. Thelen, “Shear Wave Predictions of Achilles Tendon Loading during Human Walking,” *Sci. Rep.*, vol. 9, no. 1, p. 13419, Dec. 2019, doi: 10.1038/s41598-019-49063-7.

- [3] A. J. Reiter, J. A. Martin, K. A. Knurr, and D. G. Thelen, “Shear wave tensiometry predictions of Achilles tendon force during running,” in *North American Congress on Biomechanics*, 2022.
- [4] J. Brum, M. Bernal, J. L. Gennisson, and M. Tanter, “In vivo evaluation of the elastic anisotropy of the human Achilles tendon using shear wave dispersion analysis,” *Phys. Med. Biol.*, vol. 59, no. 3, pp. 505–523, Feb. 2014, doi: 10.1088/0031-9155/59/3/505.
- [5] C. Helfenstein-Didier *et al.*, “In vivo quantification of the shear modulus of the human Achilles tendon during passive loading using shear wave dispersion analysis,” *Phys. Med. Biol.*, vol. 61, pp. 2485–2496, 2016.
- [6] J. L. Blank, D. G. Thelen, M. S. Allen, and J. D. Roth, “Sensitivity of the shear wave speed-stress relationship to soft tissue material properties and fiber alignment,” *J. Mech. Behav. Biomed. Mater.*, vol. 125, no. November 2021, p. 104964, 2021, doi: 10.1016/j.jmbbm.2021.104964.
- [7] J. A. Martin, D. G. Schmitz, A. C. Ehlers, M. S. Allen, and D. G. Thelen, “Calibration of the Shear Wave Speed-Stress Relationship in Ex Vivo Tendons,” *J. Biomech.*, vol. 90, pp. 9–15, 2019, doi: 10.1016/j.jbiomech.2019.04.015.Calibration.
- [8] E. M. Keuler, I. F. Loegering, J. A. Martin, J. D. Roth, and D. G. Thelen, “Shear Wave Predictions of Achilles Tendon Loading during Human Walking,” *Sci. Rep.*, vol. 9, no. 1, pp. 1–9, 2019, doi: 10.1038/s41598-019-49063-7.
- [9] S. E. Harper, R. A. Roembke, J. D. Zunker, D. G. Thelen, and P. G. Adameczyk, “Wearable tendon kinetics,” *Sensors (Switzerland)*, vol. 20, no. 17, pp. 1–16, 2020, doi: 10.3390/s20174805.
- [10] S. E. Harper, D. G. Schmitz, P. G. Adameczyk, and D. G. Thelen, “Fusion of Wearable Kinetic and Kinematic Sensors to Estimate Triceps Surae Work during Outdoor Locomotion on Slopes,” *Sensors*, vol. 22, no. 4, 2022, doi: 10.3390/s22041589.
- [11] D. G. Schmitz *et al.*, “Modulation of Achilles tendon force with load carriage and exosuit assistance,” *Sci. Robot.*, vol. 1514, 2022.
- [12] J. L. Blank, D. G. Thelen, and J. D. Roth, “Ligament Shear Wave Speeds Are Sensitive to Tensiometer-Tissue Interactions: A Parametric Modeling Study,” in *Computer Methods, Imaging and Visualization in Biomechanics and Biomedical Engineering: Selected Papers from the 16th International Symposium CMBBE and 4th Conference on Imaging and Visualization, August 14-16, 2019, New York City, USA*, vol. 36, 2020, pp. 48–59.
- [13] S. A. Maas, B. J. Ellis, G. A. Ateshian, and J. A. Weiss, “FEBio: Finite Elements for Biomechanics,” *J. Biomech. Eng.*, vol. 134, no. 1, pp. 011005: 1–10, Jan. 2012, doi: 10.1115/1.4005694.
- [14] J. Weiss, B. Maker, and S. Govindjee, “Finite element implementation of incompressible, transversely isotropic hyperelasticity,” *Comput. Methods Appl. Mech. Engrg.*, vol. 135, pp. 107–128, 1996.

- [15] M. Mooney, "A theory of large elastic deformation," *J. Appl. Phys.*, vol. 11, no. 9, pp. 582–592, 1940, doi: 10.1063/1.1712836.
- [16] J. C. Gardiner and J. A. Weiss, "Subject-specific finite element models can predict strain in the human medial collateral ligament," *J. Orthop. Res.*, vol. 21, pp. 1098–1106, 2003, doi: 10.1016/S0736-0266(03)00113-X.
- [17] J. A. Weiss, J. C. Gardiner, and C. Bonifasi-Lista, "Ligament material behavior is nonlinear, viscoelastic and rate-independent under shear loading," *J. Biomech.*, vol. 35, no. 7, pp. 943–950, 2002, doi: 10.1016/S0021-9290(02)00041-6.
- [18] R. W. Ogden, G. Saccomandi, and I. Sgura, "Fitting hyperelastic models to experimental data," *Comput. Mech.*, vol. 34, no. 6, pp. 484–502, 2004, doi: 10.1007/s00466-004-0593-y.
- [19] Z. Sun *et al.*, "Multidirectional mechanical properties and constitutive modeling of human adipose tissue under dynamic loading," *Acta Biomater.*, vol. 129, pp. 188–198, Jul. 2021, doi: 10.1016/j.actbio.2021.05.021.
- [20] J. Blank, M. Blomquist, L. Arant, S. Cone, and J. Roth, "Characterizing musculoskeletal tissue mechanics based on shear wave propagation - a systematic review of current methods and reported measurements," *Ann. Biomed. Eng.*, 2022, doi: 10.1007/s10439-022-02935-y.
- [21] I. Cespedes, Y. Huang, J. Ophir, and S. Spratt, "Methods for estimation of subsample time delays of digitized echo signals.," *Ultrason. Imaging*, vol. 17, no. 2, pp. 142–171, 1995, doi: 10.1006/uimg.1995.1007.
- [22] E. Maksuti, E. Widman, D. Larsson, M. W. Urban, M. Larsson, and A. Bjällmark, "Arterial Stiffness Estimation by Shear Wave Elastography: Validation in Phantoms with Mechanical Testing," *Ultrasound Med. Biol.*, vol. 42, no. 1, pp. 308–321, 2016, doi: 10.1016/j.ultrasmedbio.2015.08.012.
- [23] N. C. Rouze, Y. Deng, C. A. Trutna, M. L. Palmeri, and K. R. Nightingale, "Characterization of Viscoelastic Materials Using Group Shear Wave Speeds," *IEEE Trans. Ultrason. Ferroelectr. Freq. Control*, vol. 65, no. 5, pp. 780–794, 2018, doi: 10.1109/TUFFC.2018.2815505.
- [24] M. Bernal, I. Nenadic, M. W. Urban, and J. F. Greenleaf, "Material property estimation for tubes and arteries using ultrasound radiation force and analysis of propagating modes," *J. Acoust. Soc. Am.*, vol. 129, no. 3, pp. 1344–1354, 2011, doi: 10.1121/1.3533735.
- [25] S. P. Timoshenko, "X. On the transverse vibrations of bars of uniform cross-section," *London, Edinburgh, Dublin Philos. Mag. J. Sci.*, vol. 43, no. 253, pp. 125–131, Jan. 1922, doi: 10.1080/14786442208633855.
- [26] F. Fidanza, A. Keys, and J. T. Anderson, "Density of Body Fat in Man and Other Mammals," *J. Appl. Physiol.*, vol. 6, pp. 252–256, 1953.
- [27] F. Fidanza, "Body fat in adult man: Semicentenary of fat density and skinfolds," *Acta Diabetol.*, vol. 40, no. SUPPL. 1, pp. 242–245, 2003, doi: 10.1007/s00592-003-0076-0.

- [28] S. Sadeghi and D. H. Cortes, “Measurement of the shear modulus in thin-layered tissues using numerical simulations and shear wave elastography,” *J. Mech. Behav. Biomed. Mater.*, vol. 102, no. October 2019, p. 103502, 2020, doi: 10.1016/j.jmbbm.2019.103502.
- [29] T. M. Nguyen, M. Couade, J. Bercoff, and M. Tanter, “Assessment of viscous and elastic properties of sub-wavelength layered soft tissues using shear wave spectroscopy: Theoretical framework and in vitro experimental validation,” *IEEE Trans. Ultrason. Ferroelectr. Freq. Control*, vol. 58, no. 11, pp. 2305–2315, 2011, doi: 10.1109/TUFFC.2011.2088.
- [30] P. A. Pękala *et al.*, “The twisted structure of the Achilles tendon unraveled: A detailed quantitative and qualitative anatomical investigation,” *Scand. J. Med. Sci. Sport.*, vol. 27, no. 12, pp. 1705–1715, 2017, doi: 10.1111/sms.12835.
- [31] J. L. Blank, D. G. Thelen, and J. D. Roth, “Shear wave speeds track axial stress in porcine collateral ligaments,” *J. Mech. Behav. Biomed. Mater.*, vol. 105, no. January, p. 103704, 2020, doi: 10.1016/j.jmbbm.2020.103704.
- [32] Z. Sun, B. D. Gepner, P. S. Cottler, S. H. Lee, and J. R. Kerrigan, “In vitro mechanical characterization and modeling of subcutaneous adipose tissue: A comprehensive review,” *J. Biomech. Eng.*, vol. 143, no. 7, pp. 1–9, 2021, doi: 10.1115/1.4050286.

## Adjacent Tissues Reduce Shear Wave Speeds in Axially Loaded Tendons – *Supplementary Materials*

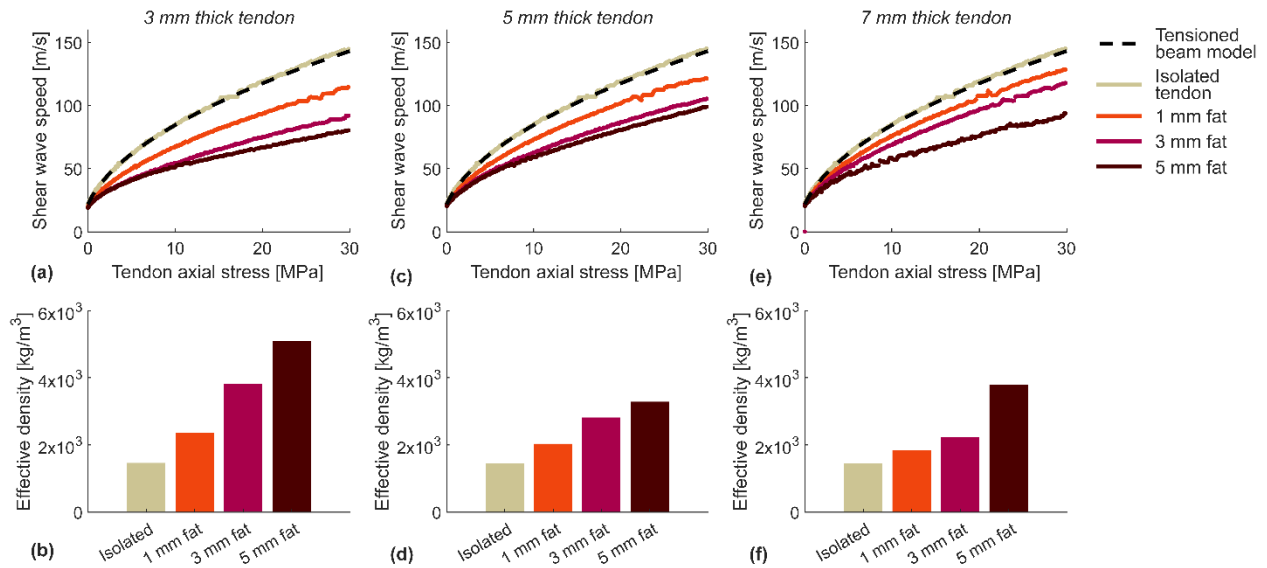


**Figure 1S:** Tendon-measured shear wave speeds were sensitive to the geometry of the tendon and subcutaneous fat, with lower shear wave speeds being measured in models with less subcutaneous fat. Isolated tendon shear wave speeds were in range of the tensioned beam model. The model conditions are as follows: **(a,b)** 3 mm thick tendon with varying subcutaneous fat thickness. **(c,d)** 5 mm thick tendon with varying subcutaneous fat thickness. **(e,f)** 7 mm thick tendon with varying subcutaneous fat thickness.